ÉCOLE POLYTECHNIQUE FÉDÉRALE DE LAUSANNE

MATHICSE

Mathematics Institute of Computational Science and Engineering

School of Basic Sciences - Section of Mathematics

MATHICSE Technical Report

Nr. 15.2014

March 2014

An anisotropic adaptive finite element algorithm for transonic viscous flows around a wing

Wissam Hassan, Marco Picasso

http://mathicse.epfl.ch

Phone: +41 21 69 37648

Address:
EPFL - SB - MATHICSE (Bâtiment MA)
Station 8 - CH-1015 - Lausanne - Switzerland

Fax: +41 21 69 32545

An anisotropic adaptive finite element algorithm for transonic viscous flows around a wing

Wissam Hassan[1a], Marco Picasso[a]

[a]*MATHICSE, Station 8, EPFL, 1015 Lausanne, Switzerland*

Abstract

An adaptive finite element algorithm to compute transonic viscous flows around a wing is presented. The adaptive criteria is based on an anisotropic error estimator in the H^1 semi-norm, justified for an advection-diffusion problem with stabilized finite elements. The mesh aspect ratio can be arbitrarly large, upper and lower bounds can be proved, the involved constants being aspect ratio independent.

Based on this error estimator, an anisotropic mesh adaptation algorithm is proposed to compute transonic viscous flows around a wing. The mesh is structured around the wing, while the remaining part of the mesh is adapted according to the anisotropic error estimator. This anisotropic adaptive algorithm allows shocks and the wake to be captured accurately, while keeping the number of vertices as low as possible.

Keywords:
advection-diffusion, a posteriori error estimator, anisotropic mesh adaptation, transonic viscous flow

1. Introduction

Adaptivity with strongly anisotropic meshes is particularly suited to solving partial differential equations with internal or boundary layers. The use of strongly anisotropic meshes involves several theoretical and practical issues: design of stable discretization methods [1], error estimates involving constants which do not depend on the mesh aspect ratio [2, 3, 4, 5, 6], convergence of solvers [7], generation of anisotropic meshes [8, 9, 10, 11]. The possible gain in memory and computing time is so important that previously intractable problems may become tractable [12].

[1]supported by Dassault Aviation

The set of partial differential equations corresponding to transonic viscous flows is therefore a good candidate to be solved with anisotropic meshes, due to the presence of both boundary layers and shocks. Strongly anisotropic structured meshes are already widely used in the aeronautic industry for the numerical simulation of transonic viscous bodies [13, 14, 15]. However, the computation of transonic flows on anisotropic structured meshes around the body and anisotropic unstructured adaptive meshes elsewhere, see figure 1, has only been tackled recently [16, 17]; it is precisely the goal of this paper.

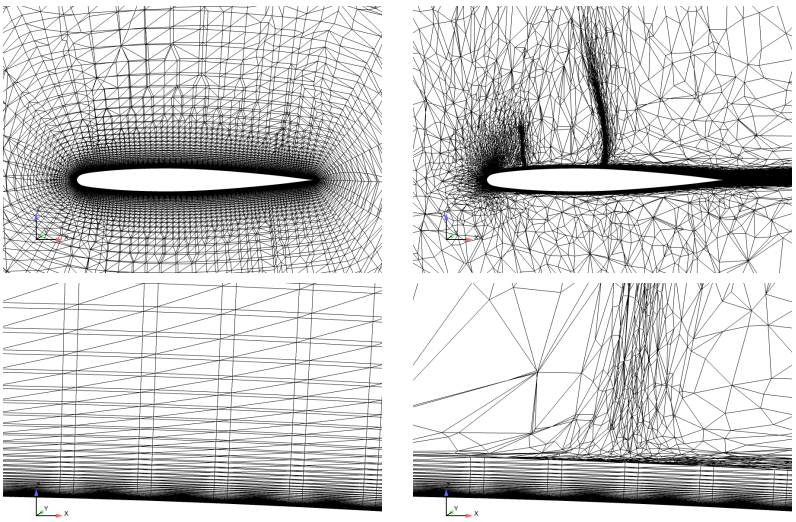

Figure 1: Examples of anisotropic meshes for transonic viscous flows around a wing. Left: structured mesh, right: structured mesh around the wing, adapted mesh elsewhere. Bottom: close view around the wing, at the intersection between the shock and the boundary layer.

The outline of the paper is the following. An anisotropic error estimator is presented for a diffusion-convection model problem in the next Section. Upper and lower bounds can be proved, the involved constants being aspect ratio independent. In Section 3, the viscous transonic flow around the ONERA M6 wing, at Reynolds number $11.72e6$, Mach number 0.84 and incident angle 3.06^o is described. Numerical results are presented on industrial non-adapted anisotropic meshes provided by Dassault Aviation. Finally, an adaptive algorithm based on the anisotropic error estimator of Section 2 is proposed. The mesh is kept structured and anisotropic around the wing, while the remaining part of the mesh is adapted according to the anisotropic error estimator. Numerical results with such anisotropic adapted meshes are then presented.

2. A model problem: advection-diffusion

An advection-diffusion model problem is introduced in order to justify the use of our adaptive criterion. For the sake of clarity, this model problem is presented in two space dimensions; it can easily be extended in three space dimensions, all the numerical experiments in this paper being in three space dimensions.

Let Ω be a polygon of $\mathbb{R}^2$, with boundary $\partial\Omega$, let $\epsilon > 0$ be the diffusion coefficient, $\mathbf{a} = (a_1, a_2)^T \in \mathbb{R}^2$ the constant velocity field, $f \in L^2(\Omega)$ the source term. We are searching for $u : \Omega \to \mathbb{R}$ such that:

$$\begin{cases} -\epsilon\,\Delta u + \mathbf{a}\cdot\nabla u = f & \text{in} \quad \Omega, \\ u = 0 & \text{on} \quad \Gamma_1, \\ \nabla u.\mathbf{n} = 0 & \text{on} \quad \Gamma_2. \end{cases} \tag{1}$$

Here we have set $\partial\Omega = \Gamma_1 \cup \Gamma_2$ with $\Gamma_1 \cap \Gamma_2 = \emptyset$, Γ_1 has non zero measure and $\mathbf{n}$ is the unit outer normal. Assuming $\mathbf{a}\cdot\mathbf{n} = 0$ on Γ_2, we have

$$\int_\Omega (\mathbf{a}\cdot\nabla u)u = 0,$$

thus the Lions-Lax-Milgram theorem applies and the above problem has a unique weak solution $u \in V = \{v \in H^1(\Omega); v = 0 \text{ on } \Gamma_1\}$. For all $h > 0$, consider $\mathcal{T}_h$ a conformal mesh of $\overline{\Omega}$ into triangles K with diameter h_K less than h. In this paper, anisotropic triangles are used, that is to say triangles with possibly large aspect ratio. The framework of [3, 4] is used to describe the mesh anisotropy, although the one of [2] could also be used. Let $T_K : \hat{K} \to K$ be the affine mapping from the reference triangle $\hat{K}$ to an arbitrary triangle K. For any $\hat{\mathbf{x}} \in \hat{K}$, let $\mathbf{x} \in K$ be the corresponding vector in triangle K defined by

$$\mathbf{x} = T_K(\hat{\mathbf{x}}) = M_K\hat{\mathbf{x}} + \mathbf{t}_K, \tag{2}$$

where $\mathbf{t}_K \in \mathbb{R}^2$ and M_K is the jacobian matrix. Since M_K is invertible, it admits a singular value decomposition

$$M_K = R_K^T \Lambda_K P_K, \tag{3}$$

where R_K and P_K are orthogonal matrices and Λ_K is a diagonal matrix with positive entries :

$$\Lambda_K = \begin{pmatrix} \lambda_{1,K} & 0 \\ 0 & \lambda_{2,K} \end{pmatrix} \quad \text{and} \quad R_K = \begin{pmatrix} \mathbf{r}_{1,K}^T \\ \mathbf{r}_{2,K}^T \end{pmatrix}, \tag{4}$$

having chosen $\lambda_{1,K} \geq \lambda_{2,K}$. The unit vectors $\mathbf{r}_{1,K}$ and $\mathbf{r}_{2,K}$ correspond to the directions of maximum and minimum stretching, the scalars $\lambda_{1,K}$ and

$\lambda_{2,K}$ correspond to the amplitudes of maximum and minimum stretching. In the framework of anisotropic meshes, the ratio between $\lambda_{1,K}$ and $\lambda_{2,K}$ can be large, however, the number of neighbours of a given vertex of the mesh should be bounded above. Moreover, due to the use of Clément interpolant, there is a technical condition involving Δ_K, the union of triangles sharing a vertex with K, see [18] for instance; this condition is satisfied whenever the variations in the direction of stretching are smooth throughout the mesh.

Let V_h be the finite element subspace of V corresponding to continuous, piecewise linear functions on the triangles of $\mathcal{T}_h$. The following stabilized finite element formulation is considered: find $u_h \in V_h$ such that

$$\begin{aligned}\int_\Omega \epsilon\, \nabla u_h \cdot \nabla v_h + \int_\Omega \mathbf{a}\cdot\nabla u_h\, v_h + \sum_{K\in\mathcal{T}_h} \tau_K \int_K (\mathbf{a}\cdot\nabla u_h)(\mathbf{a}\cdot\nabla v_h) \\ = \int_\Omega f\, v_h + \sum_{K\in\mathcal{T}_h} \tau_K \int_K f(\mathbf{a}\cdot\nabla v_h), \qquad \forall v_h \in V_h.\end{aligned} \tag{5}$$

The definition of the stabilization parameter τ_K has to be updated in order to comply with mesh anisotropy. Rather than the usual definition for isotropic meshes [19], the theoretical and numerical study performed in [1] have shown that the following choice yields accurate results:

$$\tau_K = \frac{\lambda_{2,K}}{2|\mathbf{a}|_\infty} \min(1, Pe_K) \tag{6}$$

with $|\mathbf{a}|_\infty = \max(|a_1|, |a_2|)$, Pe_K the Péclet number:

$$Pe_K = \frac{|\mathbf{a}|_\infty \lambda_{2,K}}{6\epsilon}. \tag{7}$$

In order to define our error estimator, we need some more notations. The L^2 projection onto the piecewise constants needs to be introduced; for any $K \in \mathcal{T}_h$, let

$$\Pi_K f = \frac{1}{|K|}\int_K f, \tag{8}$$

and let $|\ell_{i,K}|$, $i = 1, 2, 3$ be the three lengths of edges of K. Then, the anisotropic error estimator in the H^1 semi-norm is defined on triangle K by

$$\begin{aligned}\eta_K^2 =& \left(\frac{1}{\epsilon} \|\Pi_K f - \mathbf{a}\cdot\nabla u_h\|_{L^2(K)} + \frac{1}{2}\sum_{i=1}^{3} \left(\frac{|\ell_{i,K}|}{\lambda_{1,K}\lambda_{2,K}}\right)^{1/2} \|[\nabla u_h \cdot \mathbf{n}]\|_{L^2(\ell_{i,K})} \right) \\ & \times \omega_K (u - u_h),\end{aligned} \tag{9}$$

where $[\cdot]$ denotes the jump of the inside value across an internal edge, $[\cdot] = 0$ if the edge belongs to Γ_1, $[\cdot]$ equals twice the inside value if the edge belongs to Γ_2. Also, for all $v \in H^1(\Omega)$, for all $K \in \mathcal{T}_h$, $\omega_K(v)$ is defined by

$$(\omega_K(v))^2 = \lambda_{1,K}^2 \left(\mathbf{r}_{1,K}^T G_K(v) \mathbf{r}_{1,K}\right) + \lambda_{2,K}^2 \left(\mathbf{r}_{2,K}^T G_K(v) \mathbf{r}_{2,K}\right), \tag{10}$$

where $G_K(v)$ is the symmetric positive semi-definite matrix of first order derivatives in the patch Δ_K:

$$G_K(v) = \begin{pmatrix} \displaystyle\int_{\Delta_K} \left(\frac{\partial v}{\partial x_1}\right)^2 dx & \displaystyle\int_{\Delta_K} \frac{\partial v}{\partial x_1}\frac{\partial v}{\partial x_2} dx \\ \displaystyle\int_{\Delta_K} \frac{\partial v}{\partial x_1}\frac{\partial v}{\partial x_2} dx & \displaystyle\int_{\Delta_K} \left(\frac{\partial v}{\partial x_2}\right)^2 dx \end{pmatrix}. \tag{11}$$

The following result is a slight modification of [20] for the upper bound and an extension of [18] for the lower bound. The interested reader is referred to [21] for the full proof.

Theorem 1. *Let u be the weak solution of (1), let u_h be the solution of (5) and let η_K^2 be defined by (9). Then, there exists C_1 independent of the data f, ϵ, $\mathbf{a}$, of the mesh size and aspect ratio such that*

$$\|\nabla(u - u_h)\|_{L^2(\Omega)}^2 \leq C_1 \left(\sum_{K \in \mathcal{T}_h} \eta_K^2 + \sum_{K \in \mathcal{T}_h} \frac{\lambda_{1,K}^2}{\epsilon^2} \|f - \Pi_K f\|_{L^2(K)}^2 \right). \tag{12}$$

Moreover, if there exists C_2 independent of the mesh size and aspect ratio such that, for all $v \in H^1(\Omega)$, for all $K \in \mathcal{T}_h$:

$$\lambda_{1,K}^2 \left(\mathbf{r}_{1,K}^T G_K(v) \mathbf{r}_{1,K}\right) \leq C_2 \lambda_{2,K}^2 \left(\mathbf{r}_{2,K}^T G_K(v) \mathbf{r}_{2,K}\right), \tag{13}$$

then there exists C_3 independent of the data f, ϵ, $\mathbf{a}$, of the mesh size and aspect ratio such that

$$\begin{aligned} \sum_{K \in \mathcal{T}_h} \eta_K^2 \leq C_3 \Bigg(& \sum_{K \in \mathcal{T}_h} \|\nabla(u - u_h)\|_{L^2(\Delta_K)}^2 \left(\frac{|\mathbf{a}|_\infty \lambda_{2,K}}{\epsilon} + 1 \right) \\ & + \sum_{K \in \mathcal{T}_h} \frac{\lambda_{2,k}^2}{\epsilon^2} \|f - \Pi_K f\|_{L^2(K)}^2 \Bigg). \end{aligned} \tag{14}$$

Remark 1. *The error estimator (9) is not a usual one since u is still involved in the term $\omega_K(u - u_h)$. However, this term can be estimated efficiently using the celebrated Zienkiewicz-Zhu post-processing [22, 23], which can be justified*

whenever superconvergence occurs, see for instance [24] for a recent result in the framework of anisotropic meshes. The use of Zienkiewicz-Zhu post-processing to estimate $\omega_K(u-u_h)$ has shown to be successful in [20, 18, 25, 26]. More precisely, in $\omega_K(u-u_h)$, the term:

$$\frac{\partial u}{\partial x_j} - \frac{\partial u_h}{\partial x_j} \quad \textit{is replaced by} \quad I_h\frac{\partial u_h}{\partial x_j} - \frac{\partial u_h}{\partial x_j}, \quad j=1,2, \tag{15}$$

where $I_h\partial u_h/\partial x_j \in V_h$ and is defined, at a given vertex P of the mesh, by the average value of the neighbouring triangles:

$$I_h\frac{\partial u_h}{\partial x_j}(P) = \frac{1}{\displaystyle\sum_{\substack{K\in\mathcal{T}_h\\ P\in K}} |K|} \sum_{\substack{K\in\mathcal{T}_h\\ P\in K}} |K| \left(\frac{\partial u_h}{\partial x_j}\right)_{|K}, \quad j=1,2. \tag{16}$$

Please note that most of the error estimators used for anisotropic mesh adaptation involve an estimate of the second derivatives of u rather than the first derivatives of $u-u_h$, see for instance [27].

Remark 2. *Our error estimator is not robust in the sense of [28]; however, as soon as vertices are placed in the boundary layer, it is robust, which is precisely what will be observed in the numerical experiments.*

Numerical experiments are presented in three space dimensions. Let $\Omega = [0,1]^3$, $\mathbf{a} = (1,0,0)^T$, $f=0$, the boundary conditions are reported in figure 2, the exact solution is

$$u(x,y,z) = \frac{e^{x/\epsilon} - e^{1/\epsilon}}{1-e^{1/\epsilon}}, \tag{17}$$

thus there is a boundary layer of width ϵ at $x=1$.

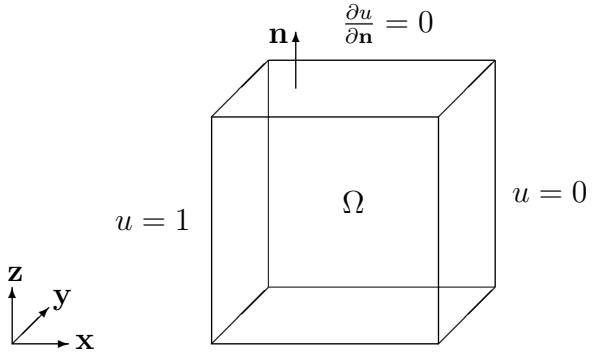

Figure 2: *Boundary conditions.*

In order to assess the accuracy of our error estimator, we define the effectivity index:

$$ei = \frac{\left(\sum_{K\in\mathcal{T}_h} \eta_K^2\right)^{1/2}}{||\nabla(u-u_h)||_{L^2(\Omega)}}.$$

Also, in order to check the accuracy of the Zienkiewicz-Zhu post-processing, we define:

$$ei^{ZZ} = \frac{\left(\int_\Omega |\nabla u_h - I_h \nabla u_h|^2\right)^{1/2}}{||\nabla(u-u_h)||_{L^2(\Omega)}}.$$

A structured mesh of Ω is considered with N_x, N_y, N_z subdivisions along each direction, see figure 3.

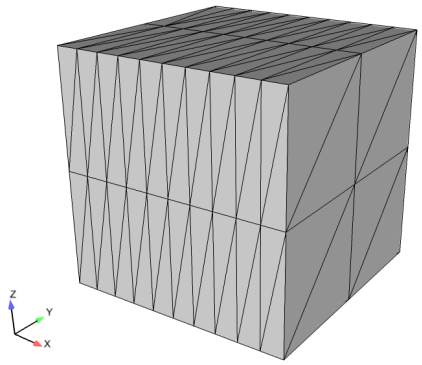

Figure 3: *A structured* $10 \times 2 \times 2$ *anisotropic mesh.*

Numerical results are reported in table 1 when $\epsilon = 0.01$ (resp. $\epsilon = 0.001$) and aspect ratio 50 (resp. 500). It can be observed that the error is decreased by a factor two each time N_x, N_y and N_z are multiplied by two, thus the error is $O(h)$. Moreover, the Zienkiewicz-Zhu effectivity index is close to one and the effectivity index of our error estimator does not depend on the aspect ratio.

$N_x \times N_y \times N_z$	$\left(\sum_{K\in\mathcal{T}_h} \eta_K^2\right)^{1/2}$	$\left(\int_\Omega \lvert\nabla(u-u_h)\rvert^2\right)^{1/2}$	ei^{ZZ}	ei	vertices
$100 \times 2 \times 2$	3.051	1.780	0.834	2.139	909
$200 \times 4 \times 4$	1.884	0.961	0.939	2.437	5025
$400 \times 8 \times 8$	1.043	0.497	0.982	2.607	32481
$800 \times 16 \times 16$	0.544	0.252	0.996	2.681	231489
$1000 \times 2 \times 2$	9.608	5.627	0.834	2.131	9009
$2000 \times 4 \times 4$	5.955	3.035	0.939	2.436	50025
$4000 \times 8 \times 8$	3.345	1.569	0.982	2.640	324081

Table 1: Numerical results when $\epsilon = 0.01$ (rows 1-4, aspect ratio 50) and $\epsilon = 0.001$ (rows 5-7, aspect ratio 500).

3. High Reynolds compressible flows around bodies

The flow of a viscous, compressible, heat conducting fluid around a wing is considered. The mass, momentum and energy conservation equations are:

$$\left\{\begin{array}{rcl} \dfrac{\partial \rho}{\partial t} + \nabla.\,(\rho \mathbf{u}) &=& 0\,, \\ \dfrac{\partial(\rho \mathbf{u})}{\partial t} + \nabla.\,(\rho \mathbf{u} \otimes \mathbf{u}) &=& \nabla.\,(\tau - pI), \\ \dfrac{\partial(\rho E)}{\partial t} + \nabla.\,(\rho E \mathbf{u}) &=& \nabla.\,\big((\tau - pI)\mathbf{u} - \mathbf{q}\big), \end{array}\right. \tag{18}$$

with ρ the density, $\mathbf{u}$ the velocity, E the total energy $E = e + \frac{||\mathbf{u}||^2}{2} + k$, e is the specific internal energy, k the turbulent kinetic energy, $p = (\gamma - 1)\rho e$ the pressure, and $T = \frac{\gamma - 1}{R} e$ the temperature ($\gamma = 1.4$), where R is a constant defined as the ideal gas constant divided by the molar mass of the gas. The heat flux $\mathbf{q}$ and the viscous tensor τ are defined by

$$\mathbf{q} = -\kappa \Delta T \qquad \text{and} \qquad \tau = \mu_t \left(\nabla \mathbf{u} + (\nabla \mathbf{u})^T\right) - \frac{2}{3}(\mu_t \nabla.\,\mathbf{u} + \rho k) I,$$

where κ is the thermal conductivity and a RANS (Reynolds Averaged Navier-Stokes) model is used to compute the turbulent viscosity μ_t:

$$\mu_t = \rho C_\mu \frac{k^2}{\epsilon}.$$

Here C_μ is a parameter and ϵ the dissipation of turbulent energy. A two-layer $k - \epsilon$ model is used [29]. The turbulent kinetic energy k satisfies

$$\frac{\partial(\rho k)}{\partial t} + \nabla \cdot (\rho \mathbf{u} k) - \nabla \cdot \left(\left(\mu + \frac{\mu_t}{\sigma_k}\right) \nabla k\right) = P_k - \frac{2}{3}\rho k \nabla \cdot \mathbf{u} - \rho \epsilon, \tag{19}$$

where σ_k is a parameter and P_k is defined by

$$P_k = \mu_t \left(\nabla \mathbf{u} + \nabla \mathbf{u}^T\right) : \nabla \mathbf{u} - \mu_t \frac{2}{3} (\nabla \cdot \mathbf{u})^2.$$

In the turbulent region, ϵ satisfies an equation similar to (19), whereas in the viscous region, ϵ is given by an algebraic relation, see [29] for details.

The ONERA M6 wing at Reynolds number $11.72e6$, Mach number 0.84 and incident angle 3.06^o is considered [30]. The computations have been performed using the AETHER Dassault Aviation code [31, 15] on various parallel clusters using the MPI library, with at most 5000 iterations. It should be stressed that the AETHER code is based on stabilized finite element formulations that allow the use of strongly anisotropic meshes and is therefore particularly well suited for anisotropic mesh adaptation. The wing is placed inside a half sphere, the mesh is produced by Dassault Aviation mesh generators; it is structured around the wing, unstructured (isotropic) elsewhere; the mesh aspect ratio is large close to the wing, up to 10 000, see figure 4. Three non-adapted meshes having smallest meshsize at the wing $1mm$, $0.1mm$ and $0.005mm$ have been used. In the structured region around the wing, the vertices are placed along the normal direction from a sequence with geometric progression 1.15; the mesh having smallest meshsize $1mm$ has a structured region made out of 30 layers, the mesh having smallest meshsize $0.1mm$ has a structured region made out of 45 layers, the mesh having smallest meshsize $0.005mm$ has a structured region made out of 70 layers. The corresponding numerical results are reported in figures 5 and 6; the Mach number in figure 5 and the pressure coefficient

$$C_P = \frac{p - P_\infty}{\frac{1}{2}\rho_\infty u_\infty^2},$$

in figure 6, where P_∞, ρ_∞ and u_∞ are the pressure, density and velocity at infinity. Accurate results are obtained when using the finest mesh. In the sequel, we will keep a structured mesh around the wing (smallest meshsize $0.005mm$, geometric progression 1.15, 40 structured layers) and adapt the mesh only outside this structured mesh.

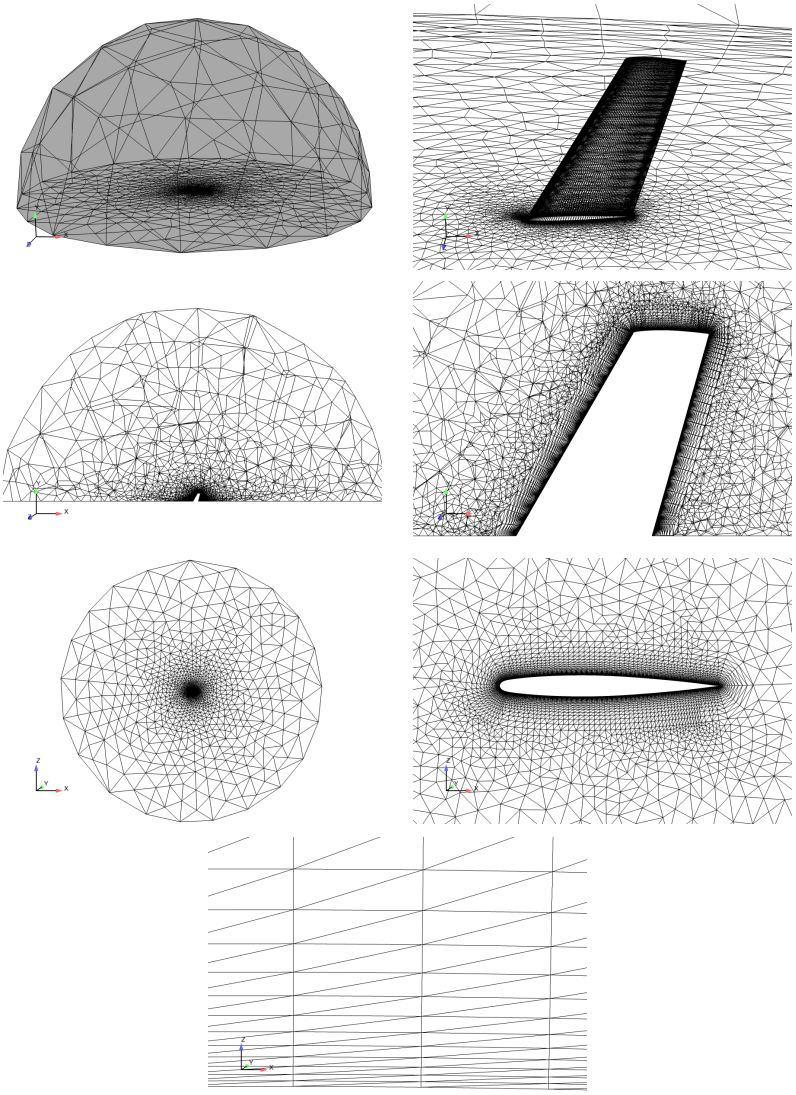

Figure 4: A typical mesh generated by Dassault Aviation. Here the mesh size at the wing, along the normal direction is $1mm$ (it is $0.005mm$ on the finest mesh); the other vertices in the structured region are placed along the normal direction according to a sequence with geometric progression 1.15.

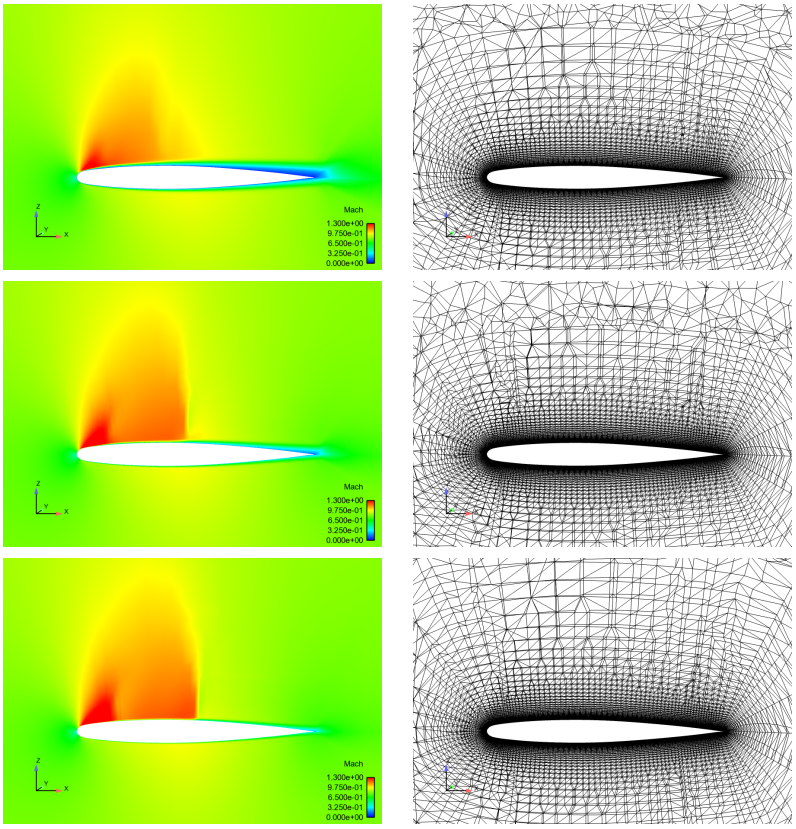

Figure 5: Cut at $y = 0.7m$ of the Mach number and mesh with three meshes having smallest mesh size at the wing $1mm$ (top), $0.1mm$ (middle) and $0.005mm$ (bottom).

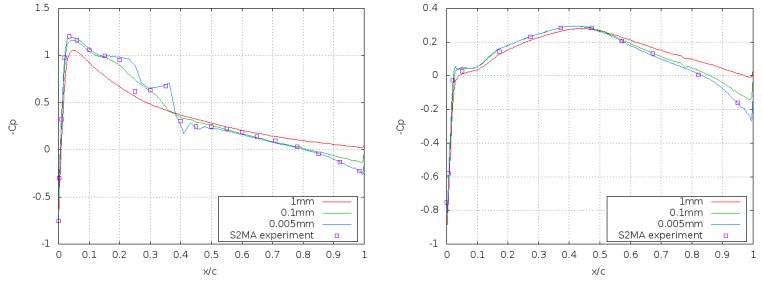

Figure 6: Pressure coefficient along the wing at $y = 957.03$ (80% of the wing); left: top of the wing, right: bottom of the wing.

4. An anisotropic, adaptive algorithm

Our goal is to build an anisotropic mesh for which the relative estimated error is close to a preset tolerance TOL:

$$\frac{\left(\sum_{K\in\mathcal{T}_h^{ext}} \eta_K^2\right)^{\frac{1}{2}}}{||\nabla M_h||_{L^2(\Omega^{ext})}} \approx TOL.$$

Here Ω^{ext} is the part of the computational domain Ω that does not contain a preset structured mesh of the boundary layer; $\mathcal{T}_h^{ext}$ is a mesh of Ω^{ext}. Also, M_h is the computed Mach number corresponding to the exact one:

$$M = \frac{\|\mathbf{u}\|}{\sqrt{\gamma RT}} = \frac{\|\mathbf{u}\|}{\sqrt{\gamma p/\rho}}.$$

The error estimator η_K is defined by:

$$\eta_K^2 = \frac{1}{2}\sum_{i=1}^{4}\left(\frac{|f_{i,K}|}{\lambda_{1,K}\lambda_{2,K}\lambda_{3,K}}\right)^{1/2} \|[\nabla M_h\cdot\mathbf{n}]\|_{L^2(f_{i,K})}\,\omega_K(M-M_h), \qquad (20)$$

where $f_{i,K}$ is a face of tetrahedron K and $\omega_K(M-M_h)$ is defined by:

$$(\omega_K(M-M_h))^2 = \sum_{i=1}^{3}\lambda_{i,K}^2\left(\mathbf{r}_{i,K}^T G_K(M-M_h)\mathbf{r}_{i,K}\right).$$

Here $G_K(v)$ is the 3×3 matrix of first order derivatives defined as in (11), $\mathbf{r}_{1,K}$, $\mathbf{r}_{2,K}$, $\mathbf{r}_{3,K}$ and $\lambda_{1,K}$, $\lambda_{2,K}$, $\lambda_{3,K}$ are defined as in (3) (4), Zienkiewicz-Zhu post-processing is used to estimate $\omega_K(M-M_h)$, as explained in Remark 1.

The reader should note that this error estimator is similar to the one presented in the inviscid case [32]. Going back to (9), only the term corresponding to the jump of the normal gradient has been kept. This choice led to excellent results for various elliptic, parabolic and hyperbolic problems [18, 33, 26] and has been justified in [2] in the elliptic case. We have decided to use $\omega_K(M-M_h)$ rather than $\omega_K(\mathbf{u}-\mathbf{u}_h)$ since most of the informations (shock and boundary layers) are contained in the Mach number M. A theoretical justification of such a choice would be needed but is missing. Indeed, to our knowledge, there are no a posteriori error estimates for the compressible Navier-Stokes equations; an existence result for (18) without the $k-\epsilon$ model has been proved only recently in [34].

In order to implement (20), a mesh $\mathcal{T}_h^{ext}$ is generated such that

$$0.75^2\, TOL^2 ||\nabla M_h||^2_{L^2(\Omega^{ext})} \leq \sum_{K\in\mathcal{T}_h^{ext}} \eta_K^2 \leq 1.25^2\, TOL^2 ||\nabla M_h||^2_{L^2(\Omega^{ext})}. \quad (21)$$

A sufficient condition to build such a mesh is to enforce, for each tetrahedron $K \in \mathcal{T}_h^{ext}$:

$$\frac{0.75^2 TOL^2 ||\nabla M_h||^2_{L^2(\Omega^{ext})}}{N_K^{ext}} \leq \eta_K^2 \leq \frac{1.25^2 TOL^2 ||\nabla M_h||^2_{L^2(\Omega^{ext})}}{N_K^{ext}}.$$

where N_K^{ext} is the total number of tetrahedrons of $\mathcal{T}_h^{ext}$. The `MMG3D` anisotropic remesher is used to build $\mathcal{T}_h^{ext}$ [8]. Given a metric $\mathcal{M}(P)$ at each vertex P of the mesh, the `MMG3D` remesher builds a new mesh consistent with this metric. We now explain how to compute this metric.

For each vertex P of the mesh, let η_P^4 be the error estimator at vertex P defined by:

$$\eta_P^4 = \sum_{\substack{K\in\mathcal{T}_h^{ext}\\ P\in K}} \eta_K^4.$$

We split the error into the three stretching directions:

$$\eta_K^4 = \eta_{K,1}^4 + \eta_{K,2}^4 + \eta_{K,3}^4$$

where $\eta_{K,i}^4$ is the error estimator in direction $\mathbf{r}_{i,K}$, $i = 1, 2, 3$:

$$\eta_{K,i}^4 = \left(\frac{1}{2} \sum_{j=1}^{4} \left(\frac{|f_{j,K}|}{\lambda_{1,K}\lambda_{2,K}\lambda_{3,K}} \right)^{\frac{1}{2}} ||[\nabla M_h.\mathbf{n}]||_{L^2(f_{j,K})} \right)^2 \lambda_{i,K}^2 (\mathbf{r}_{i,K}^T G_K (M - M_h)\mathbf{r}_{i,K}).$$

The error estimator in direction i and vertex P is now defined by:

$$\eta_{P,i}^4 = \sum_{\substack{K\in\mathcal{T}_h^{ext}\\ P\in K}} \eta_{K,i}^4 \qquad \text{and} \quad \eta_P^4 = \eta_{P,1}^4 + \eta_{P,2}^4 + \eta_{P,3}^4.$$

Then

$$\sum_{P\in\mathcal{T}_h} \eta_P^4 = 4 \sum_{K\in\mathcal{T}_h} \eta_K^4,$$

so that a sufficient condition to satisfy (21) is to insure, for each vertex P of the mesh $\mathcal{T}_h^{ext}$:

$$\frac{\sqrt{4}}{N_P^{ext}} 0.75^2 TOL^2 ||\nabla M_h||^2_{L^2(\Omega^{ext})} \leq \eta_P^2 \leq \frac{\sqrt{4}}{N_P^{ext}} 1.25^2 TOL^2 ||\nabla M_h||^2_{L^2(\Omega^{ext})},$$

N_P^{ext} being the number of vertices in $\mathcal{T}_h^{ext}$. The two above inequalities are satisfied when

$$\frac{4}{3\,(N_P^{ext})^2} 0.75^4 TOL^4 ||\nabla M_h||^4_{L^2(\Omega^{ext})} \leq \eta^4_{P,i} \leq \frac{4}{3\,(N_P^{ext})^2} 1.25^4 TOL^4 ||\nabla M_h||^4_{L^2(\Omega^{ext})}, \quad (22)$$

for $i = 1, 2, 3$. The algorithm used to build the requested metric $\mathcal{M}(P)$ at each vertex P of $\mathcal{T}_h^{ext}$ is then the following. For each vertex P of the mesh, we compute $G_P(M - M_h)$, and average value of $G_K(M - M_h)$ on the tetrahedrons K surrounding P :

$$G_P(M - M_h) = \frac{\displaystyle\sum_{\substack{K \in \mathcal{T}_h \\ P \in K}} G_K(M - M_h)}{\displaystyle\sum_{\substack{K \in \mathcal{T}_h \\ P \in K}} 1},$$

where Zienkiewicz-Zhu post-processing has been used to estimate $G_K(M - M_h)$. We then compute an orthonormal basis $Q_P(M - M_h)$ of the eigenvectors of $G_P(M - M_h)$. Our goal is to align the tetrahedrons around vertex P with the eigenvectors of $G_P(M - M_h)$. Thus, the metric is defined by

$$Q_P^T \begin{pmatrix} \frac{1}{h_{1,P}^2} & 0 & 0 \\ 0 & \frac{1}{h_{2,P}^2} & 0 \\ 0 & 0 & \frac{1}{h_{3,P}^2} \end{pmatrix} Q_P, \quad (23)$$

where the desired mesh size at vertex P, $h_{1,P}$, $h_{2,P}$, $h_{3,P}$, is prescribed in order to satisfy (22). Let $\lambda_{i,P}$, $i = 1, 2, 3$, be an average value of $\lambda_{i,K}$ on the tetrahedrons K surrounding P. If

$$\frac{4}{3(N_P^{ext})^2} 0.75^4 TOL^4 \|\nabla M_h\|^4_{L^2(\Omega^{ext})} > (\eta_{P,i})^4,$$

then the values of $h_{i,P}$ are set to $2\lambda_{i,P}$, $i = 1, 2, 3$, if

$$\frac{4}{3(N_P^{ext})^2} 0.75^4 TOL^4 \|\nabla M_h\|^4_{L^2(\Omega^{ext})} \leq (\eta_{P,i})^4 \leq \frac{4}{3(N_P^{ext})^2} 1.25^4 TOL^4 \|\nabla M_h\|^4_{L^2(\Omega^{ext})},$$

then the values of $h_{i,P}$ are set to $\lambda_{i,P}$, $i = 1, 2, 3$, if

$$(\eta_{P,i})^4 > \frac{4}{3(N_P^{ext})^2} 1.25^4 TOL^4 \|\nabla M_h\|^4_{L^2(\Omega^{ext})},$$

then the values of $h_{i,P}$ are set to $\lambda_{i,P}/2$, $i = 1, 2, 3$.

5. Numerical results with adapted meshes

Consider a structured mesh around the wing having smallest mesh size at the wing $0.005mm$, geometric progression 1.15, 40 structured layers. The adaptive algorithm is run with $TOL = 2$, the results after 0, 5, 10, 15 mesh iterations are reported in figure 7. The pressure coefficient is reported in figure 8. Although the adapted mesh is refined across the shocks and the wake, the initial (non-adapted) mesh yields the most accurate pressure coefficient. This indicates that the TOL parameter should be further decreased. The number of vertices and the average mesh anisotropy are reported with respect to the mesh iteration number in figure 9. The required number of mesh iterations to observe mesh convergence is between 5 and 10.

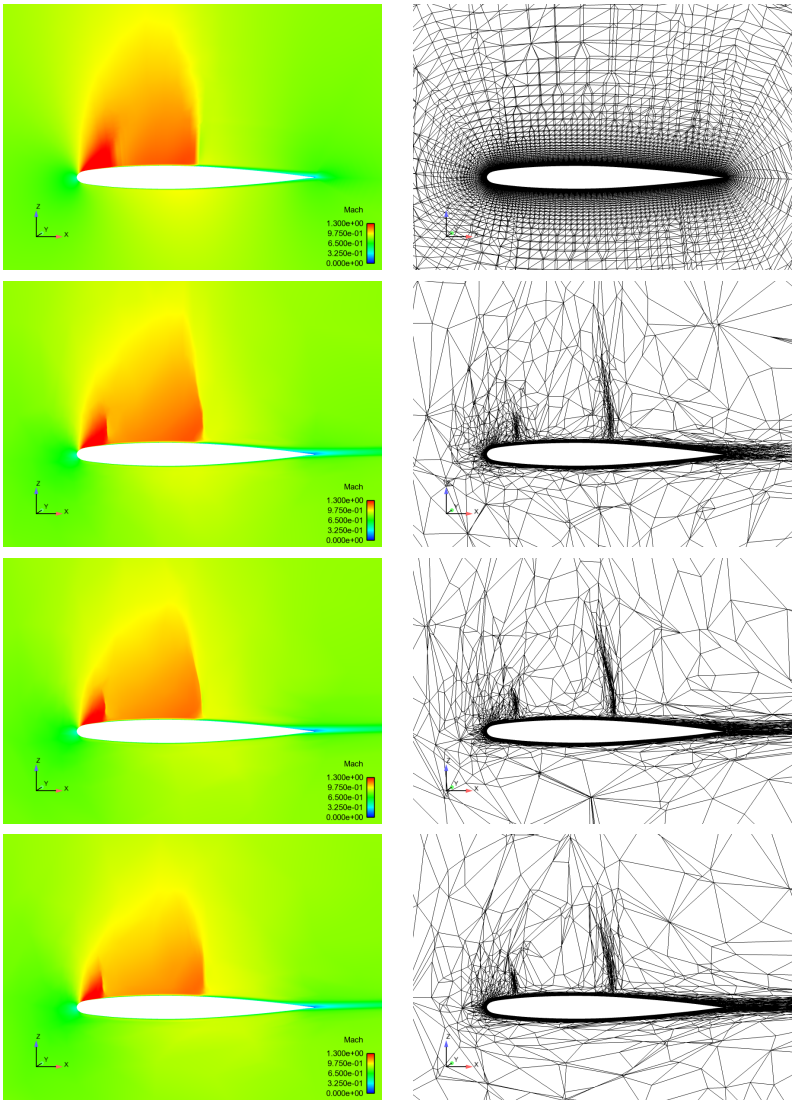

Figure 7: *Cut at $y = 0.7m$ of the adapted mesh when running the adaptive algorithm with $TOL = 2$. Mach number (left column) and mesh (right column). First row: initial mesh, second to fourth row: after 5, 10 and 15 mesh iterations.*

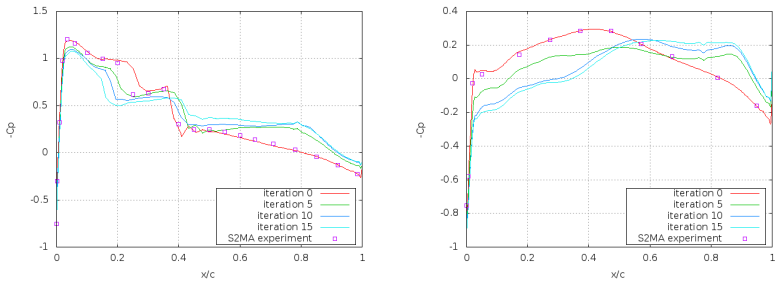

Figure 8: *Pressure coefficient along the wing at* $y = 957.03$ *(80% of the wing) when running the adaptive algorithm with* $TOL = 2$*; left: top of the wing, right: bottom of the wing.*

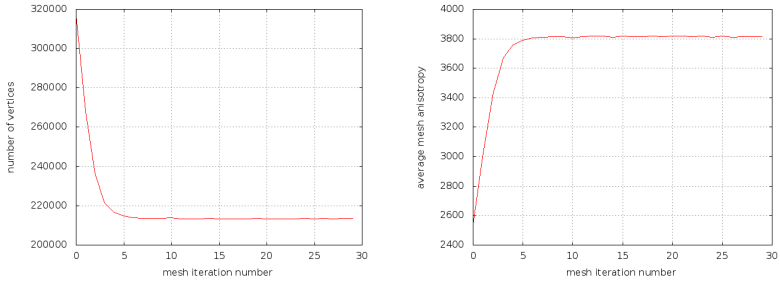

Figure 9: *Number of vertices and average mesh anisotropy with respect to the mesh iteration number when running the adaptive algorithm with* $TOL = 2$*.*

Numerical results are now compared when running the adaptive algorithm with three different values of TOL, namely $TOL = 2$, $TOL = 1$, $TOL = 0.5$. The Mach number is presented after 15 mesh iterations in figure 10, the pressure coefficient in figure 11; the pressure coefficient is accurate when $TOL = 0.5$. The number of vertices and the average mesh anisotropy are reported with respect to the mesh iteration number in figure 12. When $TOL = 0.5$, the required number of mesh iterations increases. The observed convergence behaviour is the following: the mesh is first refined isotropically until iteration 10, then coarsened anisotropically.

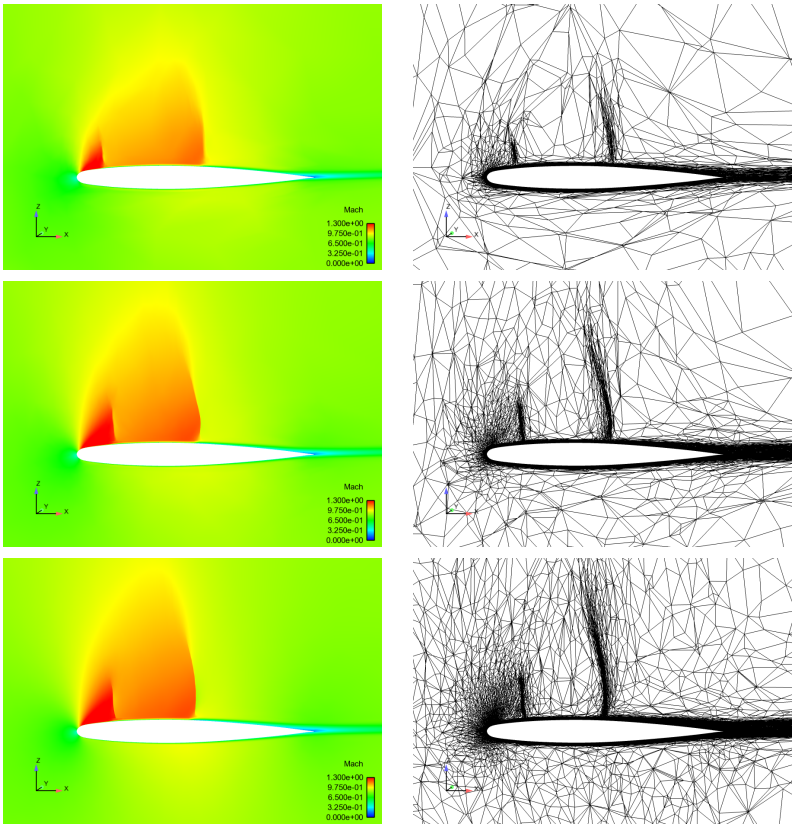

Figure 10: *Cut at* $y = 0.7m$ *of the adapted mesh when running the adaptive algorithm with three values of* TOL*. Mach number (left column) and mesh (right column). From top to bottom:* $TOL = 2$*,* $TOL = 1$ *and* $TOL = 0.5$*.*

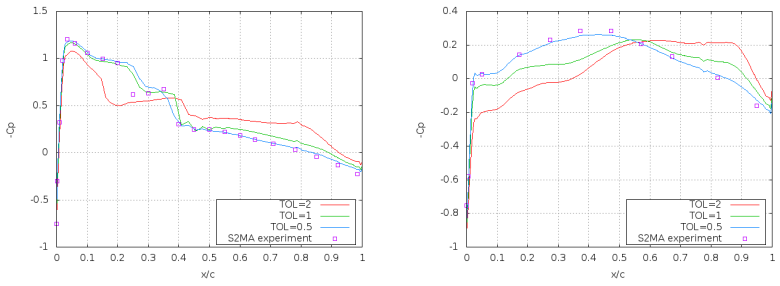

Figure 11: *Pressure coefficient along the wing at* $y = 957.03$ *(80% of the wing) when running the adaptive algorithm with* $TOL = 2$*,* $TOL = 1$ *and* $TOL = 0.5$*; left: top of the wing, right: bottom of the wing.*

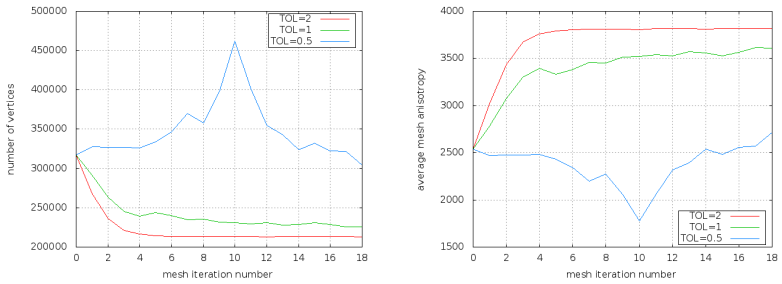

Figure 12: *Number of vertices and average mesh anisotropy with respect to the mesh iteration number when running the adaptive algorithm with* $TOL = 2$, $TOL = 1$ *and* $TOL = 0.5$.

Finally, we have compared the solution on the initial non-adapted mesh and on the final adapted mesh ($TOL = 0.5$, 15 mesh iterations). Both meshes have a similar number of vertices, 317005 on the initial mesh, 304539 on the adapted mesh. Although the pressure coefficient along the wing is similar, the shocks and wake are better captured on the adapted mesh. Figures 13-16 contain the relevant comparisons. We therefore conclude that a goal oriented anisotropic error estimator is preferable to obtain a better accuracy on the pressure coefficient. We refer to [35] for a goal oriented anisotropic error estimator in the framework of the advection-diffusion problem, to [14] for goal oriented anisotropic error estimation and adaptivity in 2D compressible viscous flows and to [36] for goal oriented anisotropic adaptivity in 3D compressible inviscid flows. Preliminar results of the present method on the ONERA M6 wing with a goal oriented anisotropic error estimator can be found in [21].

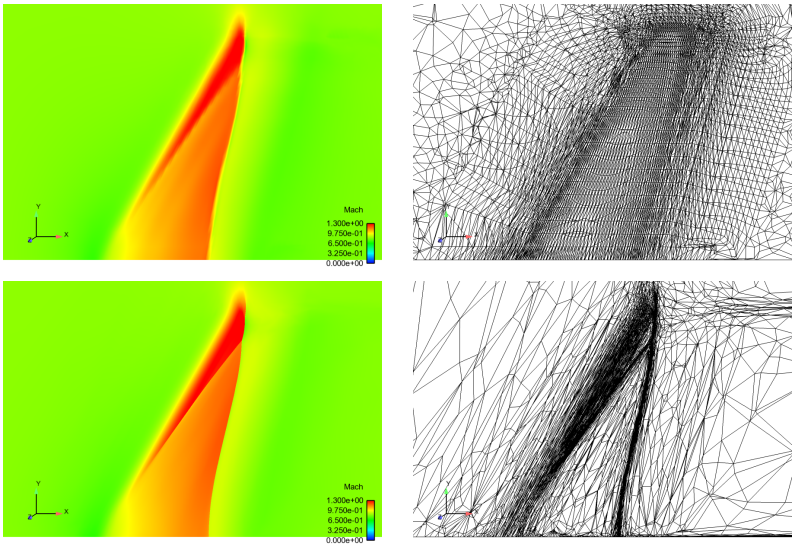

Figure 13: *Cut at* $z = 0.08m$ *of the mesh and Mach number. Top: initial non-adapted mesh, bottom: final adapted mesh with* $TOL = 0.5$.

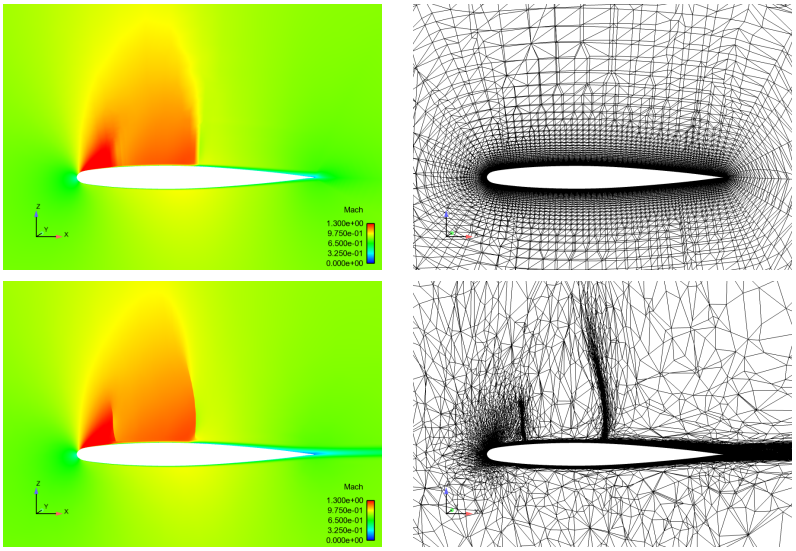

Figure 14: *Cut at* $y = 0.7m$ *of the mesh and Mach number. Top: initial non-adapted mesh, bottom: final adapted mesh with* $TOL = 0.5$.

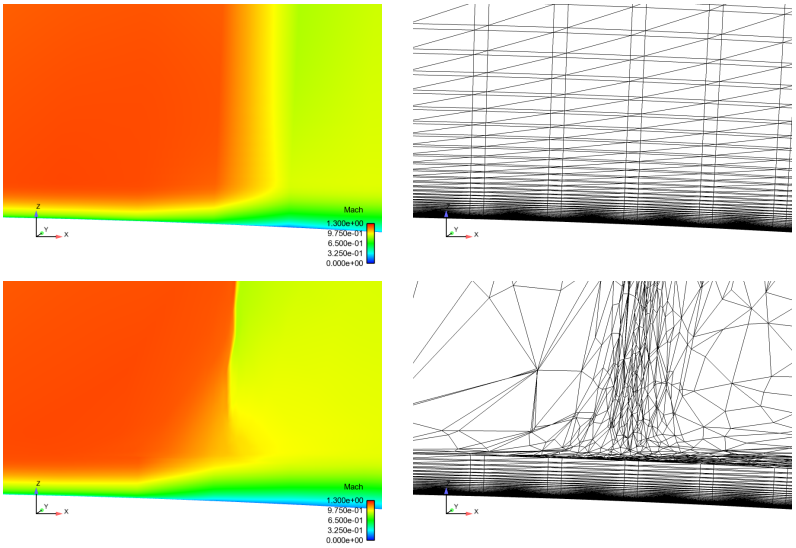

Figure 15: *Zoom at the main shock.*

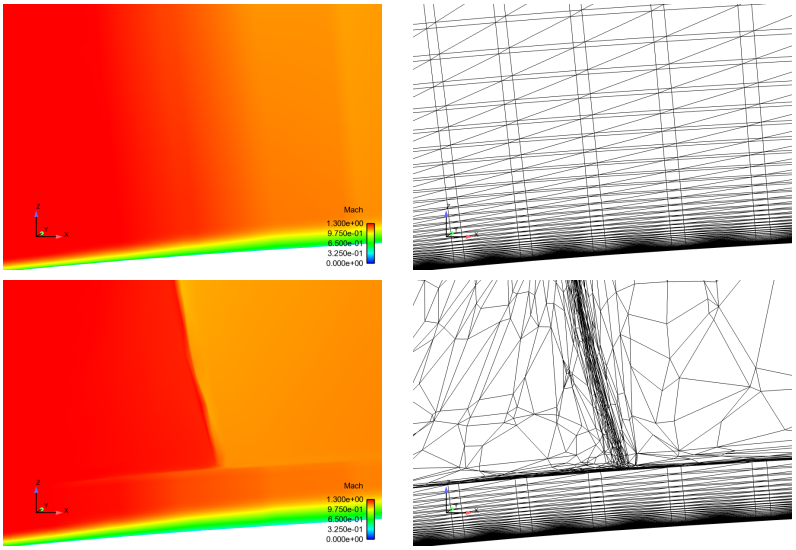

Figure 16: *Zoom at the secondary shock.*

6. Conclusions

An anisotropic, a posteriori error estimator for the H^1 semi-norm of the error has been presented for a convection-diffusion problem. The equivalence between the error and the estimator can be proved. Numerical results on

a 3D boundary layer problem indicate that the effectivity index does not depend on the mesh aspect ratio.

An anisotropic, adaptive algorithm based on this error estimator is proposed in the framework of a transonic viscous flow around the ONERA M6 wing. A structured layer of tetrahedrons is kept in the boundary layer around the wing, the mesh is adapted anisotropically outside this structured layer. The shocks and wake are described with great accuracy.

Focusing on the pressure coefficient along the wing, numerical results indicate that a goal oriented error estimator is needed. Moreover, a structured adaptation in the boundary layer is also needed to capture with great precision the interaction between the shock and the boundary layer. This will be the subject of a future research.

7. Acknowledgements

The authors would like to thank Didier Alleau, Jean-Pierre Figeac, Nicolas Flandrin, Alain Naïm and Gilbert Rogé from Dassault Aviation for their support during this work.

Cécile Dobrzynski and Pascal Frey are acknowledged for providing the `MMG3D` anisotropic remesher.

References

[1] S. Micheletti, S. Perotto, M. Picasso, Stabilized finite elements on anisotropic meshes: a priori error estimates for the advection-diffusion and the stokes problems, SIAM Journal on Numerical Analysis 41 (3) (2003) 1131–1162.

[2] G. Kunert, R. Verfürth, Edge residuals dominate a posteriori error estimates for linear finite element methods on anisotropic triangular and tetrahedral meshes, Numerische Mathematik 86 (2000) 283–303.

[3] L. Formaggia, S. Perotto, New anisotropic a priori error estimates, Numerische Mathematik 89 (2001) 641–667.

[4] L. Formaggia, S. Perotto, Anisotropic error estimates for elliptic problems, Computing and Visualization in Science 4 (2001) 99–104.

[5] A. Loseille, F. Alauzet, Continuous mesh framework part I: well-posed continuous interpolation error, SIAM J. Numer. Anal. 49 (1) (2011) 38–60.

[6] T. Coupez, Metric construction by length distribution tensor and edge based error for anisotropic adaptive meshing, J. Comput. Phys. 230 (7) (2011) 2391–2405.

[7] M. Picasso, A stopping criterion for the conjugate gradient algorithm in the framework of anisotropic adaptive finite elements, Comm. Numer. Methods Engrg. 25 (4) (2009) 339–355.

[8] C. Dobrzynski, Adaptation de maillage anisotrope 3d et application à l'aéro-thermique des bâtiments, Ph.D. thesis, Université Pierre et Marie Curie, Paris VI, France (2005).

[9] A. Loseille, F. Alauzet, Continuous mesh framework part II: validations and applications, SIAM J. Numer. Anal. 49 (1) (2011) 61–86.

[10] A. Loseille, R. Löhner, On 3d anisotropic local remeshing for surface, volume and boundary layers, in: Proceedings of the 18th International Meshing Roundtable, Springer, 2009, pp. 611–630.

[11] C. Gruau, T. Coupez, 3D tetrahedral, unstructured and anisotropic mesh generation with adaptation to natural and multidomain metric, Comput. Methods Appl. Mech. Engrg. 194 (48-49) (2005) 4951–4976.

[12] E. Hachem, S. Feghali, R. Codina, T. Coupez, Immersed stress method for fluid-structure interaction using anisotropic mesh adaptation, Internat. J. Numer. Methods Engrg. 94 (9) (2013) 805–825.

[13] M. A. Park, D. L. Darmofal, Parallel anisotropic tetrahedral adaptation, in: AIAA Paper, Vol. 917, 2008.

[14] T. Leicht, R. Hartmann, Error estimation and anisotropic mesh refinement for 3d laminar aerodynamic flow simulations, J. Comput. Phys. 229 (19) (2010) 7344–7360.

[15] F. Chalot, Industrial aerodynamics, in: Encyclopedia of Computational Mechanics, Edited by Erwin Stein, René de Borst and Thomas J.R. Hughes. Volume 3: Fluids, John Wiley & Sons, Ltd, 2004, pp. 407–458.

[16] A. Loseille, R. Löhner, Anisotropic adaptive simulations in aerodynamics, in: AIAA Paper, Vol. 169, 2010.

[17] A. Loseille, R. Lohner, Boundary layer mesh generation and adaptivity, in: 49th AIAA Aerospace Sciences Meeting including the New Horizons Forum and Aerospace Exposition, 2011.

[18] M. Picasso, Adaptive finite elements with large aspect ratio based on an anisotropic error estimator involving first order derivatives, Computer Methods in Applied Mechanics and Engineering 196 (2006) 14–23.

[19] L. Franca, S. Frey, T. Hugues, Stabilized finite element methods: I. application to the advective-diffusive model, Computer Methods in Applied Mechanics and Engineering 95 (1992) 253–276.

[20] M. Picasso, An anisotropic error indicator based on zienkiewicz-zhu error estimator: application to elliptic and parabolic problems, SIAM Journal on Scientific Computing 24 (4) (2003) 1328–1355.

[21] W. Hassan, Algorithmes d'adaptation de maillages anisotropes et application à l'aérodynamique, Ph.D. thesis, EPFL, number 5304, `http://library.epfl.ch/theses` (2012).

[22] O. Zienkiewicz, J. Zhu, A simple error estimator and adaptive procedure for practical engineering analysis, International Journal for Numerical Methods in Engineering 24 (1987) 337–357.

[23] M. Ainsworth, J. Zhu, A. Craig, O. Zienkiewicz, Analysis of the zienkiewicz-zhu a posteriori error estimator in the finite element method, International Journal for Numerical Methods in Engineering 28 (9) (1989) 2161–2174.

[24] W. Cao, Superconvergence analysis of the linear finite element method and a gradient recovery postprocessing on anisotropic meshes, Math. Comp. (2014) 2014.

[25] M. Picasso, Numerical study of an anisotropic error estimator in the $L^2(H^1)$ norm for the finite element discretization of the wave equation, SIAM J. Sci. Comput. 32 (4) (2010) 2213–2234.

[26] Y. Bourgault, M. Picasso, Anisotropic error estimates and space adaptivity for a semidiscrete finite element approximation of the transient transport equation, SIAM J. Sci. Comput. 35 (2) (2013) A1192–A1211.

[27] M. Picasso, F. Alauzet, H. Borouchaki, P.-L. George, A numerical study of some Hessian recovery techniques on isotropic and anisotropic meshes, SIAM J. Sci. Comput. 33 (3) (2011) 1058–1076.

[28] R. Verfürth, Robust a posteriori error estimates for stationary convection-diffusion equations, SIAM J. Numer. Anal. 43 (4) (2005) 1766–1782.

[29] P. Durbin, Turbulence closure models for computational fluid dynamics, Encyclopedia of Computational Mechanics 3 (2004) 301–324.

[30] V. Schmitt, F. Charpin, Pressure distribution on the onera m6 wing at transonic mach numbers, in: Experimental Data Base for Computer Program Assessment, Report of the Fluid Dynamics Panel Working Group 04, AGARD AR 138, 1979.

[31] F. Chalot, M. Mallet, M. Ravachol, A comprehensive finite element navier-stokes solver for low-and high-speed aircraft design, in: AIAA paper, no. 0814, 1994.

[32] Y. Bourgault, M. Picasso, F. Alauzet, A. Loseille, On the use of anisotropic a posteriori error estimators for the adaptative solution of 3D inviscid compressible flows, Internat. J. Numer. Methods Fluids 59 (1) (2009) 47–74.

[33] E. Burman, M. Picasso, Anisotropic, adaptive finite elements for the computation of a solutal dendrite, J. Interfaces and Free Boundaries 5 (2003) 103–127.

[34] D. Bresch, B. Desjardins, On the existence of global weak solutions to the navier-stokes equations for viscous compressible and heat conducting fluids., Journal de Mathématiques Pures et Appliquées 87 (2007) 57–90.

[35] L. Dedè, S. Micheletti, S. Perotto, Anisotropic error control for environmental applications, Applied Numerical Mathematics 58 (2008) 1320–1339.

[36] A. Loseille, A. Dervieux, F. Alauzet, Fully anisotropic goal-oriented mesh adaptation for 3D steady Euler equations, J. Comput. Phys. 229 (8) (2010) 2866–2897.

Recent publications:

MATHEMATICS INSTITUTE OF COMPUTATIONAL SCIENCE AND ENGINEERING
Section of Mathematics
Ecole Polytechnique Fédérale
CH-1015 Lausanne

02.2014 FEDERICO NEGRI, ANDREA MANZONI, GIANLUIGI ROZZA:
Certified reduced basis method for parametrized optimal control problems governed by the Stokes equations

03.2014 CEDRIC EFFENBERGER, DANIEL KRESSNER:
On the residual inverse iteration for nonlinear eigenvalue problems admitting a Rayleigh functional

04.2014 TAKAHITO KASHIWABARA, CLAUDIA M. COLCIAGO, LUCA DEDÈ, ALFIO QUARTERONI:
Numerical Well-posedness, regularity, and convergence analysis of the finite element approximation of a generalized Robin boundary value problem

05.2014 BJÖRN ADLERBORN, BO KAGSTRÖM, DANIEL KRESSNER:
A parallel QZ algorithm for distributed memory HPC systems

06.2014 MICHELE BENZI, SIMONE DEPARIS, GWENOL GRANDPERRIN, ALFIO QUARTERONI:
Parameter estimates for the relaxed dimensional factorization preconditioner and application to hemodynamics

07.2014 ASSYR ABDULLE, YUN BAI:
Reduced order modelling numerical homogenization

08.2014 ANDREA MANZONI, FEDERICO NEGRI:
Rigorous and heuristic strategies for the apporximation of stability factors in nonlinear parametrized PDEs

09.2014 PENG CHEN, ALFIO QUARTERONI:
A new algorithm for high-dimensional uncertainty quantification problems based on dimension-adaptive and reduced basis methods

10.2014 NATHAN COLLIER, ABDUL-LATEEF HAJI-ALI, FABIO NOBILE, ERIK VON SCHWERIN, RAÚL TEMPONE:
A continuation multilevel Monte Carlo algorithm

11.2014 LUKA GRUBISIC, DANIEL KRESSNER:
On the eigenvalue decay of solutions to operator Lyapunov equations

12.2014 FABIO NOBILE, LORENZO TAMELLINI, RAÚL TEMPONE:
Convergence of quasi-optimal sparse grid approximation of Hilbert-valued functions: application to random elliptic PDEs

13.2014 REINHOLD SCHNEIDER, ANDRÉ USCHMAJEW:
Convergence results for projected line-search methods on varieties of low-rank matrices via Lojasiewicz inequality

14.2014 DANIEL KRESSNER, PETAR SIRKOVIC:
Greedy law-rank methods for solving general linear matrix equations

15.2014 WISSAM HASSAN, MARCO PICASSO:
An anisotropic adaptive finite element algorithm for transonic viscous flows around a wing